Nonuniform flow in compound channel: A 1-D method for assessing water level and discharge distribution

Sébastien Proust, D. Bousmar, N. Rivière, André Paquier, Y. Zech

Nonuniform flow in compound channel: A 1-D method for assessing water level and discharge distribution

Sébastien Proust,[1] Didier Bousmar,[2] Nicolas Riviere,[3] André Paquier,[1] and Yves Zech[4]

Received 13 May 2009; revised 29 July 2009; accepted 17 August 2009; published 16 December 2009.

[1] This paper investigates 1-D modeling of nonuniform flows in compound channels. The issue is how to accurately predict both flow depth and mean velocity in the floodplain. A new model, called "Independent Subsections Method" (ISM), is presented here. Unlike classical 1-D models that solve a dynamic equation on the total cross section, the ISM estimates the water surface profile within each subsection. This enables the water level and the subsection mean velocities to be simultaneously calculated, without priority to any variable. In opposition to the Divided Channel Method (DCM), corrected DCM or the Exchange Discharge Model, the ISM assumes independent evolution of the discharge in each subsection of the compound channel. Indeed, this method does not assume equal head loss gradients in all subsections, and it does not impose the downstream discharge distribution. The ISM consists in a set of three coupled 1-D momentum equations (written within main channel, left-hand, and right-hand floodplains) and a mass conservation equation on the total cross section. Mass and momentum exchanges at the interfaces between subsections are explicitly accounted for. This method is validated against experimental data for developing flows in straight compound channel, flows in skewed compound channel, flows in a symmetric converging or diverging compound channel, and flows in an asymmetrical compound channel with an abrupt floodplain contraction. For the 46 runs, the ISM predicts flow depth and mean velocity in the floodplain with a maximum relative error of 8% and 19%, respectively. The ISM also appears to be a useful theoretical tool to improve our understanding of physical processes governing compound channel flows.

Citation: Proust, S., D. Bousmar, N. Riviere, A. Paquier, and Y. Zech (2009), Nonuniform flow in compound channel: A 1-D method for assessing water level and discharge distribution, *Water Resour. Res.*, *45*, W12411, doi:10.1029/2009WR008202.

1. Introduction

[2] When overbank flows occur in natural rivers, they often give rise to nonuniform flows. These nonuniform flows are caused by bed level changes, longitudinal variation in channel width, and/or unbalanced discharge distribution across the channel. Putting aside the effects of bed level changes on flow, we investigate two types of flow in this paper: nonuniform flows with a constant channel width or with a variable channel width. In both cases, nonuniform flows are characterized by mass exchange between the flows in the main channel and the floodplains. This lateral mass discharge also transfers momentum when the flow velocity differs from one subsection to another. An additional momentum transfer is due to turbulent exchange at the interface between the main channel and the floodplains. The physics of flooding rivers is therefore governed by the following three different sources of energy dissipation: (1) classical bed friction; (2) momentum transfer due to interfacial turbulent exchange; and (3) momentum transfer due to mass exchange between subsections. The total momentum transfer induces additional head losses that reduce the overall channel conveyance and affect the discharge distribution across the channel and the water stage. The complexity of such nonuniform flows results from the variation in these additional head losses depending on the geometry, overall discharge, and relative flow depth (i.e., the ratio between the flow depth in the floodplains and in the main channel).

[3] The aim of the present study was to find a simple approach that is appropriate for various geometries with either constant or variable channel width, and able to accurately predict both flow depth and mean velocity in the floodplain. We restricted the investigation to 1-D approaches. One-dimensional models are useful when studying long reaches, when there is few field data for calibration, and when the topography of floodplains is not surveyed in detail.

[4] In the literature, the majority of 1-D models were validated under uniform flow conditions: formulas using the apparent shear stress concept listed by *Martin-Vide and Moreta* [2008]; the empirical corrections of the Divided Channel Method (DCM) such as formulas proposed by *Nicollet and Uan* [1979] and *Ackers* [1993]; the mixing

[1]Unité de Recherche Hydrologie-Hydraulique, Cemagref, Lyon, France.
[2]Laboratoire de Recherche Hydraulique, Service Public de Wallonie, Châtelet, Belgium.
[3]Laboratoire de Mécanique des Fluids et d'Acoustique, UMR5509, CNRS, INSA de Lyon, Villeurbanne, France.
[4]Unité de Génie Civil, Université Catholique de Louvain, Louvain-la-Neuve, Belgium.

0043-1397/09/2009WR008202$09.00

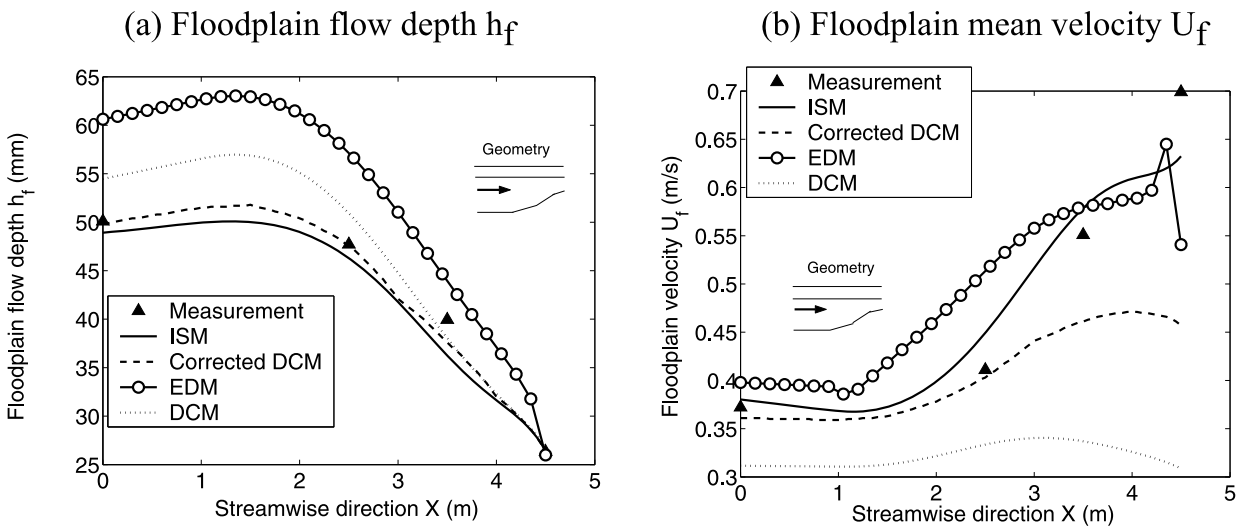

Figure 1. Abrupt floodplain contraction, relative depth $H^* \in [0.24;0.14]$. Results of DCM, corrected DCM, EDM, and ISM shown against experimental measurements.

length model developed by *Bousmar and Zech* [1999] or the formula proposed by *Huthoff et al.* [2008].

[5] To the authors knowledge, 1-D models tested under nonuniform flow conditions are few. The Exchange Discharge Model (EDM) of *Bousmar and Zech* [1999] was validated in River Sambre (Belgium) and in a flume with symmetrically narrowing floodplains [*Bousmar et al.*, 2004], focusing on the relationships between water stages and total discharge. The improved 1-D modeling developed by *Martin-Vide et al.* [2008] is appropriate for meandering compound channels with vegetated floodplains. The ability of the DCM, a corrected DCM and of the EDM to work out both flow depth and mean velocity in the floodplain for nonuniform flows was evaluated by *Bousmar* [2002], *Proust* [2005], and *Proust et al.* [2006a, 2006b]. These three 1-D methods led to moderate errors in the floodplain flow depth values (maximum relative error of 25%) and to significant errors, up to 133%, in the floodplain discharge. Figure 1 illustrates the results of these three methods for a flow in a compound channel with an abrupt floodplain contraction (mean angle of 22°). It was found that a 1-D equation defined on the total cross section cannot satisfactorily predict both flow depth and discharge distribution between subsections. The following three constraining 1-D assumptions were identified: (1) the computation of the backwater surface profile using a dynamic equation on the overall cross-section area; (2) assuming equal head loss gradients in the subsections; and (3) imposing uniform flow conditions for downstream discharge distribution.

[6] In order to cope with the problems of modeling nonuniform flows in compound channel, another type of 1-D approach is possible. It was first proposed by *Yen* [1984]. This method consists in a set of rigorously derived one-dimensional flow equations. The total cross section is subdivided into three subsections according to the changes in geometry and in roughness: the main channel, the left-hand and the right-hand floodplains. A one-dimensional momentum equation is then written on each subsection, taking into account the corresponding continuity equation formulated on the subsection. Restricting the method to a straight compound channel geometry, *Yen et al.* [1985] then proposed a backwater computation procedure. Last, they applied the method to a virtual straight compound channel, with various boundary conditions, and compared the relative weights of mass exchange and turbulent shear stress in the momentum transfer between subsections. Relying on numerical computations only, these authors showed that in comparison with mass exchange, turbulent transfers have a negligible effect on the water surface profile. To our knowledge, Yen's method was unfortunately not compared to experimental data.

[7] This paper presents the extension of the method developed by *Yen et al.* [1985] to nonprismatic compound channels with constant or variable channel width. We propose a new system of ordinary differential equations with specific treatment of interfacial exchanges. The new method is called "Independent Subsections Method" (ISM). First, we present the main hypotheses of the ISM, the flow equations and the final differential equations system. Second, we describe how the interfacial momentum transfer is modeled. Mainly, we present the calibration of turbulent exchanges under uniform flow conditions and the modeling of streamwise depth-averaged velocity at the vertical interfaces between subsections for nonuniform flows. Last, we compare ISM calculations to experimental measurements collected in four compound channel flumes: at Compagnie Nationale du Rhône (CNR), Lyon, France; at Laboratoire de Mécanique des Fluides et d'Acoustique (LMFA), Lyon, France; at Université Catholique de Louvain (UCL), Louvain-la-Neuve, Belgium; at the Hydraulic Research Center of Wallingford (Flood Channel Facility (FCF)), Wallingford, United Kingdom. The characteristics of the flumes are given in Table 1. Eleven various geometries were investigated with either constant channel width (Figure 2) or variable width (Figure 3): developing flows in straight compound channel, flows in skewed compound channel, in a symmetric converging or diverging compound channel, and in an asymmetrical compound channel with an abrupt floodplain contraction. The ISM is also used as a theoretical tool to

Table 1. Flume Characteristics for Straight Compound Geometries

Flume Name	CNR	UCL	LMFA	FCF Series A3[a]
Length L (m)	14	10	8	56
Total width B (m)	3.00	1.20	1.20	3.3
Longitudinal slope $S_0 \times 1000$	1.90	0.99	1.80	1.027
Left floodplain width B_l (m)	–	0.40	–	0.75
Right floodplain width B_r (m)	2.20	0.40	0.80	0.75
Ratio B/B_m	3.75	3	3	1.83
Bankfull depth h_b (m)	0.160	0.050	0.0515	0.150
Main channel banks slope (°)	58	90	90	45
Bed material	smoothed cement	coated plywood	PVC	smoothed cement
Manning roughness n (s/m$^{1/3}$)	0.0119–0.0132	0.0107–0.0117	0.0090–0.0093	0.0096–0.0114

[a]*Knight* [1992].

estimate the main physical processes governing compound channel flows.

2. Independent Subsections Method

[8] Our new model was named Independent Subsections Method to underline the fact that the water surface profile is estimated within each subsection. This characteristic is of primordial importance since it enables the subsection head loss gradients to be, to a certain extent, "independent."

[9] In the following, we consider compound channels composed of a main channel and two floodplains as shown in Figure 4. Subscripts "m," "l," and "r" are used for mean values of hydraulic parameters in the main channel, the left-hand floodplain and the right-hand floodplain, respectively. Subscript "f" is used for "floodplain" in general (left or/and right). Subscript "i" is used for a subsection in general ($i = m, l, r$). Two parallel subsections with regard to the streamwise direction are identified by subscripts i and "j."

2.1. Differences Between the ISM, Corrected DCM, and EDM

[10] The respective assumptions of the ISM, the corrected DCM, and the EDM are summed up in Table 2. As

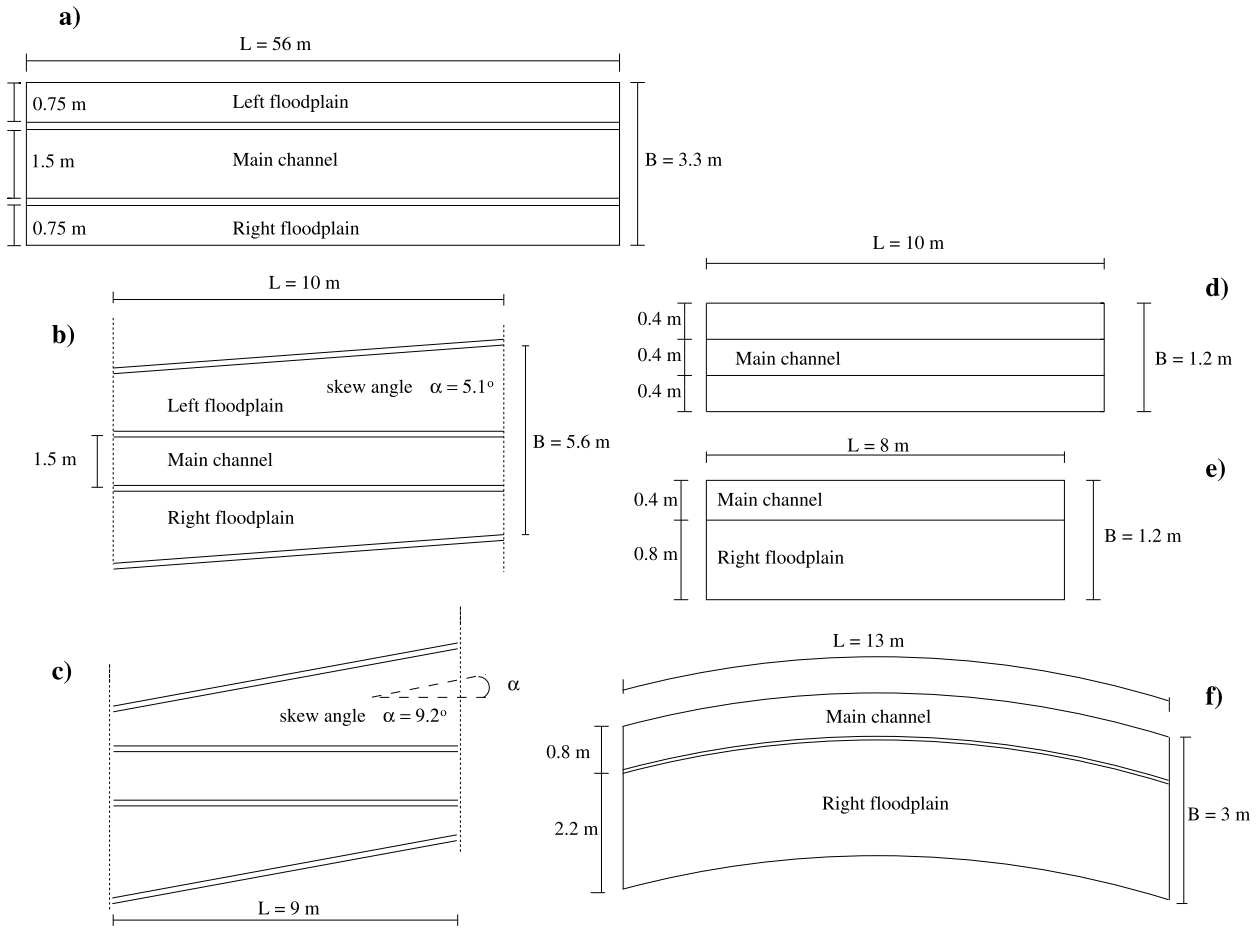

Figure 2. Top view of the compound geometries with constant total width: (a) FCF Series A3, (b and c) FCF skewed floodplains, (d) UCL flume, (e) LMFA flume, and (f) CNR flume.

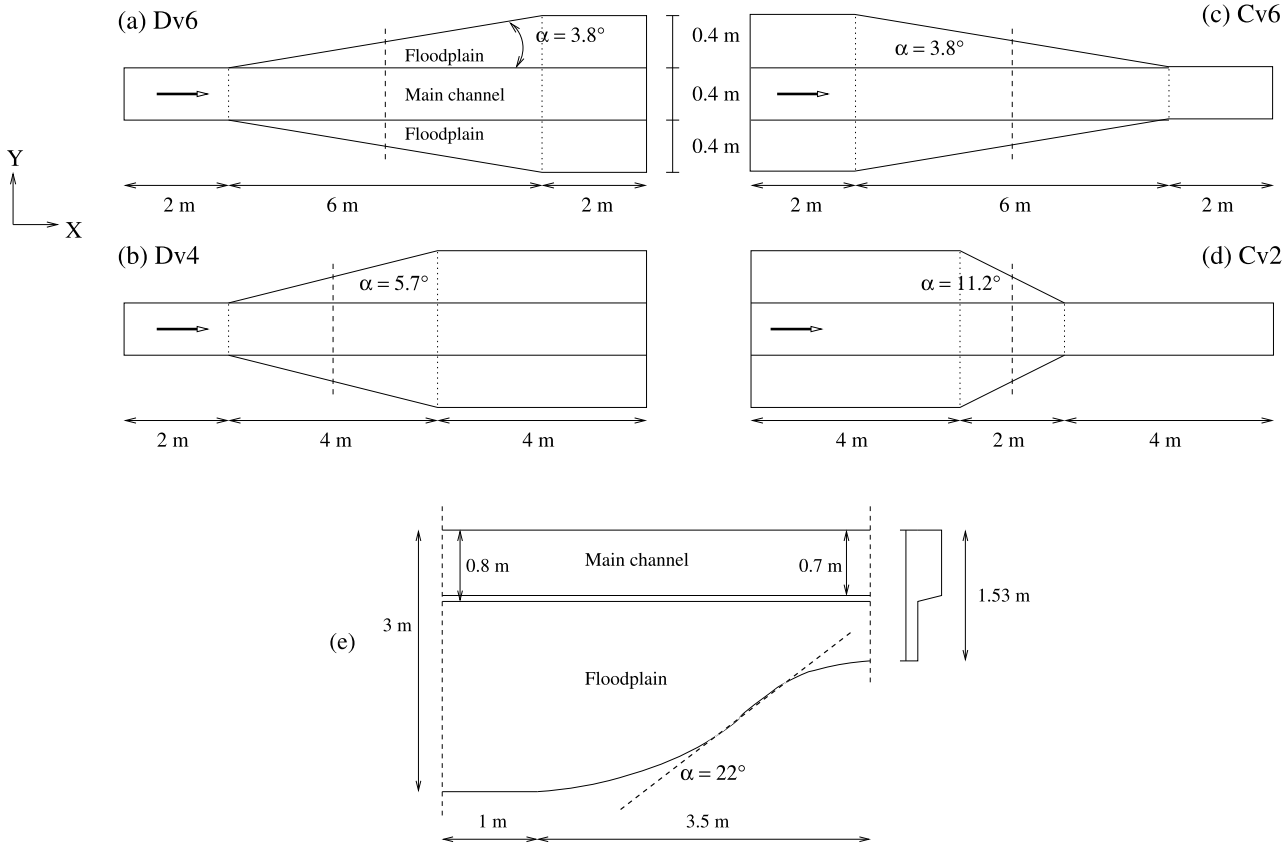

Figure 3. Top view of geometries with variable width: diverging geometries (a) Dv6 and (b) Dv4, UCL flume; converging geometries (c) Cv6 and (d) Cv2, UCL flume; and (e) abrupt floodplain contraction, CNR flume.

previously mentioned, the main novelty in the ISM is to compute the water surface profile in the subsection. This characteristic leads to the release of the following constraining assumptions of the common 1-D approaches: (1) Unlike corrected DCM or EDM that state equality between the head loss gradients in the subsections ($S_{Hm} = S_{Hf}$), these gradients are independent from one subsection to another in the ISM. (2) The ISM does not impose uniform flow conditions for the downstream discharge distribution. (3) The EDM computes bed friction slope S_f on the total cross section by using the DCM formula, which implicitly assumes equal friction slopes in the subsections ($S_{fm} = S_{ff}$); in the ISM, there is no estimation in the total cross section and no associated hypothesis. Last, the ISM considers the measured discharges Q_m and Q_f in the upstream cross section as upstream input.

2.2. ISM Equations

[11] The ISM is composed of three momentum equations. These equations are linked together by lateral mass discharges and terms of momentum transfer acting at the interface between two parallel subsections with regard to

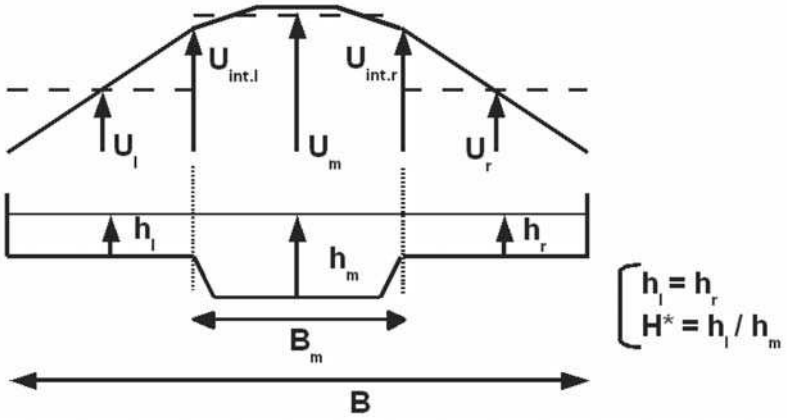

Figure 4. Notations of hydraulic and geometrical parameters.

Table 2. Respective Assumptions of the Corrected DCM, EDM, and ISM

Assumptions on	Corrected DCM	EDM	ISM
Water surface profile computed on	the whole cross section	the whole cross section	each subsection
Bed friction slope S_f computed on the whole cross section	yes	yes, using S_f computed by DCM	–
Bed friction slope S_{fi} computed in each subsection i	yes	yes	yes
Vertical shear stress τ_{ij} between two adjacent subsections i and j	empirical formulas [see, e.g., *Nicollet and Uan*, 1979; *Ackers*, 1993]	$\lvert\tau_{ij}\rvert = \rho\Psi^t\,(U_i - U_j)^2$	$\lvert\tau_{ij}\rvert = \rho\Psi^t\,(U_i - U_j)^2$
Lateral mass discharge q	–	$\lvert q\rvert = \psi^g\,\lvert dQ_f/dx\rvert$ with $0 \le \psi^g \le 1$	$\lvert q\rvert = \lvert dQ_f/dx\rvert$
Interfacial velocity U_{int}	–	partially via ψ^g	empirical formulas
Subsection head loss gradient S_{Hi}	$S_{Hm} = S_{Hf}$	$S_{Hm} = S_{Hf}$	independent
Upstream discharge distribution	–	–	actual Q_m and Q_f
Downstream discharge distribution (Q_m and Q_f)	implicitly imposed (uniform flow conditions)	implicitly imposed (uniform flow conditions)	–

longitudinal direction. An additional equation ensures mass conservation on the overall cross-section area.

[12] The subsections considered here are assumed to be rectangular and their width can vary. The interfaces between subsections are assumed to be vertical and parallel to the longitudinal direction. Moreover, the velocity is assumed to be uniform in each subsection. Under these assumptions, and for steady flow, the 1-D momentum equation in a subsection i in the x direction for a unit length gives [see *Bousmar and Zech*, 1999, equation (5)]

$$S_{fi} = S_0 - \frac{dh_i}{dx} \pm \frac{\tau_{ij}.h_{\text{int}}}{\rho g A_i} - \frac{1}{gA_i}\frac{d}{dx}\left(A_i U_i^2\right) + \frac{(U_{in}q_{in} - U_{out}q_{out})}{gA_i}, \tag{1}$$

where x is longitudinal direction; h_i is subsection flow depth; h_{int} is flow depth at the interface is h_l or h_r; U_i is subsection mean velocity; A_i is subsection area; S_o is bed slope; S_{fi} is subsection friction slope; τ_{ij} is algebraic value of the shear stress acting at the vertical interface in the x direction between subsections i and j; q_{in} (q_{out}) is the lateral mass discharge per unit longitudinal length entering (leaving) the subsection with a streamwise velocity U_{in} (U_{out}).

[13] On the right hand side of equation (1), the two last terms are related to the momentum conveyed by the lateral inflow q_{in} and the lateral outflow q_{out} through the interface between subsections. The products $U_{in}.q_{in}$ and $U_{out}.q_{out}$ are the terms of momentum flux (divided by ρ) due to mass exchange.

[14] The mass conservation in a subsection i for steady flow gives

$$\frac{dA_iU_i}{dx} = q_{in} - q_{out}, \tag{2}$$

where discharges q_{in} and q_{out} are considered positive and are mutually exclusive.

[15] In equations (1) and (2) entering lateral discharge q_{in} and exiting lateral discharge q_{out} are distinguished. In fact, only two lateral discharges should be considered: the lateral mass discharge between the right floodplain (the left floodplain) and the main channel q_{rm} (q_{lm}). Both are positive if mass is leaving the floodplains, and negative if mass is entering the floodplains, i.e., in a mathematical way: $q_{out} = q_{lm}$ and $q_{in} = 0$ in the left floodplain; $q_{out} = q_{rm}$ and $q_{in} = 0$ in the right floodplain; $q_{out} = 0$ and $q_{in} = q_{lm} + q_{rm}$ in the main channel.

[16] Equation (2) within the three subsections gives

$$\frac{dQ_l}{dx} = -q_{lm}, \tag{3}$$

$$\frac{dQ_r}{dx} = -q_{rm}, \tag{4}$$

$$\frac{dQ_m}{dx} = q_{lm} + q_{rm}, \tag{5}$$

where the sum of the subsection discharges Q_m, Q_r and Q_l, is the total discharge Q.

[17] Combining equations (3)–(5) leads to mass conservation on the whole cross-section area

$$\frac{dQ_m}{dx} + \frac{dQ_l}{dx} + \frac{dQ_r}{dx} = 0. \tag{6}$$

Combining equations (1) and (2), and isolating the flow depth gradient (see Appendix A), the 1-D momentum equations within the three subsections become

$$\left(1 - \frac{U_l^2}{gh_l}\right)\frac{dh_l}{dx} = S_o - S_{fl} + \frac{U_l^2}{gB_l}\frac{dB_l}{dx} + \frac{\tau_{lm}.h_l}{\rho g A_l} + \frac{q_{lm}(2U_l - U_{\text{int}.l})}{gA_l}, \tag{7}$$

$$\left(1 - \frac{U_r^2}{gh_r}\right)\frac{dh_r}{dx} = S_o - S_{fr} + \frac{U_r^2}{gB_r}\frac{dB_r}{dx} + \frac{\tau_{rm}.h_r}{\rho g A_r} + \frac{q_{rm}(2U_r - U_{\text{int}.r})}{gA_r}, \tag{8}$$

$$\left(1 - \frac{U_m^2}{gh_m}\right)\frac{dh_m}{dx} = S_o - S_{fm} + \frac{U_m^2}{gB_m}\frac{dB_m}{dx} - \frac{\tau_{lm}.h_l}{\rho g A_m} - \frac{\tau_{rm}.h_r}{\rho g A_m} \ldots - \frac{q_{lm}(2U_m - U_{\text{int}.l})}{gA_m} - \frac{q_{rm}(2U_m - U_{\text{int}.r})}{gA_m}, \tag{9}$$

where B_i is subsection width; τ_{ij} is shear stress at the vertical interfaces, the signs preceding τ_{ij} being appropriate for a y axis oriented from right to left; $U_{int.l}$ ($U_{int.r}$) is longitudinal velocity at the interface between the main channel and the left floodplain (the right floodplain) as shown in Figure 4. The subsection friction slope S_{fi} is calculated with the

Manning's formula applied to a subsection, or with the Darcy-Weisbach formula when the flow is not fully rough turbulent

$$S_{fi} = \frac{f_i}{4R_i}\frac{U_i^2}{2g}, \tag{10}$$

where R_i is the hydraulic radius accounting for solid walls only, and f_i is the Darcy-Weisbach coefficient.

[18] For UCL, LMFA and CNR geometry, Manning roughness was estimated by isolating the main channel from the floodplain and by using various experimental flow rates. For instance, $n_m = 0.019$ and $n_f = 0.0132$ s/m$^{1/3}$ in the CNR flume (cement slightly rougher in the floodplain). For FCF Series A3, Manning roughness were estimated from the measurements of boundary shear stress presented by *Knight* [1992]. The Manning roughness values are presented in Table 1.

[19] The 6 main unknowns are the three flow depths h_l, h_m, h_r and the three velocities U_l, U_m and U_r. The 6 secondary unknowns are the 2 shear stresses τ_{lm} and τ_{rm}, the 2 interfacial velocities $U_{int.l}$ and $U_{int.r}$, and the 2 lateral discharges q_{rm} and q_{lm}. With the three mass conservation equations (3)–(5) and the three momentum equations (7)–(9), six closure equations are required. As suggested by *Yen* [1984] and in agreement with experimental measurements, water level Z across the compound channel is assumed to be constant at a given station x, as $Z_m = Z_r = Z_l$. If h_b is the bank full depth, $h_l = h_r = h_m - h_b$, and $dh_m/dx = dh_l/dx = dh_r/dx$. The assumption $Z_l = Z_m = Z_r$ was validated against measured water level in the various geometries investigated, excepted at the end of the abrupt floodplain contraction (x = 4.5m in Figure 1). *Proust et al.* [2006a] showed that assuming equal Z_i between subsections leads to an underestimation of −9% of the floodplain velocity at x = 4.5m. The 4 remaining closure equations define the vertical shear stresses (τ_{lm} and τ_{rm}) and the velocities at the interfaces ($U_{int.l}$, $U_{int.r}$); they are presented below.

[20] The Independent Subsections Method thus consists in solving the set of ordinary differential equations (6)–(9) considering the closure equations. One flow depth and three subsection velocities are calculated simultaneously. The solving procedure is presented in appendix B. As the upstream discharge distribution has to be considered as an additional boundary condition [see *Bousmar et al.*, 2005], ISM accounts for the measured upstream total discharge and upstream discharge distribution, and the measured downstream water level.

3. Momentum Transfer at the Interfaces

[21] Using the Independent Subsections Method requires accurate modeling of the momentum transfer between two parallel subsections, as the associated terms are explicitly expressed in equations (7)–(9). As a result, interfacial shear stress due to turbulent exchange, and terms of momentum transfer due to mass exchange, have to be appropriately accounted for. Shear stresses τ_{lm} and τ_{rm} are modeled in the horizontal plane following the mixing length concept. Interface velocities $U_{int.l}$ and $U_{int.r}$ are modeled using a parameterization that relies on experimental measurements of interfacial velocity in the various geometries investigated.

3.1. Turbulent Exchange

[22] The vertical shear stress τ_{lm} or τ_{rm} are evaluated using the mixing length model in the horizontal plane. The mixing length model was validated by *Ervine and Baird* [1982], *Lambert and Sellin* [1996], and *Bousmar* [2002]. The model used in the Exchange Discharge Model (EDM) was adopted [*Bousmar and Zech*, 1999]. Here τ_{lm} and τ_{rm} are modeled by

$$|\tau_{lm}| = \rho\Psi^t(U_m - U_l)^2, \tag{11}$$

$$|\tau_{rm}| = \rho\Psi^t(U_m - U_r)^2, \tag{12}$$

where ψ^t is a constant coefficient of turbulent exchange.

[23] The coefficient of turbulent exchange ψ^t is considered to be constant in equations (11) and (12) for a given geometry even when the hydraulic parameters are varied. The ψ^t value of the ISM was calibrated under uniform flow conditions in two small-scale compound channel flumes, the LMFA and UCL flumes, and in the Flood Channel Facility for Series A3 [*Knight*, 1992] presented in Table 1.

[24] Under uniform flow conditions, equations (7)–(9) simplify, and τ_{lm}, τ_{rm} and ψ^t can be estimated from hydraulic parameters. Figure 5a presents ψ^t coefficient versus relative depth H^*, the ratio between the flow depth in the floodplains and in the main channel. Ranging from 0.014 to 0.033, the ψ^t values vary around a mean value of 0.022 in the three flumes with no clear tendency.

[25] As ISM focused on the computation of floodplain flow depth (h_f) and floodplain discharge ($Q_f = Q_l + Q_r$), a sensitivity analysis of these mean parameters to ψ^t value was carried out. Figure 5b shows results for a UCL flow with relative depth $H^* = 0.18$ and $x \in [7; 14\text{m}]$ where the uniform flow conditions are established [see *Bousmar et al.*, 2005]. Four simulations are performed: with $\psi^t = 0$ (no turbulent diffusion), $\psi^t = 0.02$ (the averaged value on the two small-scale flumes), $\psi^t = 0.03$, the calibrated value related to $H^* = 0.18$, and a arbitrary strong value $\psi^t = 0.2$, ten times bigger than the mean value.

[26] The simulated floodplain discharge Q_f is not constant if turbulent diffusion is not considered or with including the arbitrary strong value. These ψ^t values lead, respectively, to underestimation and overestimation of floodplain discharge: −18% and +34%. Computing the floodplain discharge with the mean value of 0.02 instead of the calibrated values leads to a maximum error of 6%. Moreover, the sensitivity analysis with higher relative depth showed that the effect of turbulent diffusion decreases with increasing relative depth (result not shown here). Hence, ISM simulations were performed using the turbulent exchange coefficient $\psi^t = 0.02$.

3.2. Momentum Flux Due to Mass Exchange

[27] In the equations (7)–(9), the products (q_{lm}. $U_{int.l}$) and (q_{rm}. $U_{int.r}$) are the terms of momentum flux due to mass exchange through the two interfaces. An accurate modeling of the interface velocities $U_{int.l}$ and $U_{int.r}$ is thus required when the flow is nonuniform. To model these velocities, we relied on all the data sets presented in Table 3: developing flows in straight compound channels, flows in compound channels with skewed floodplains, with symmetrically

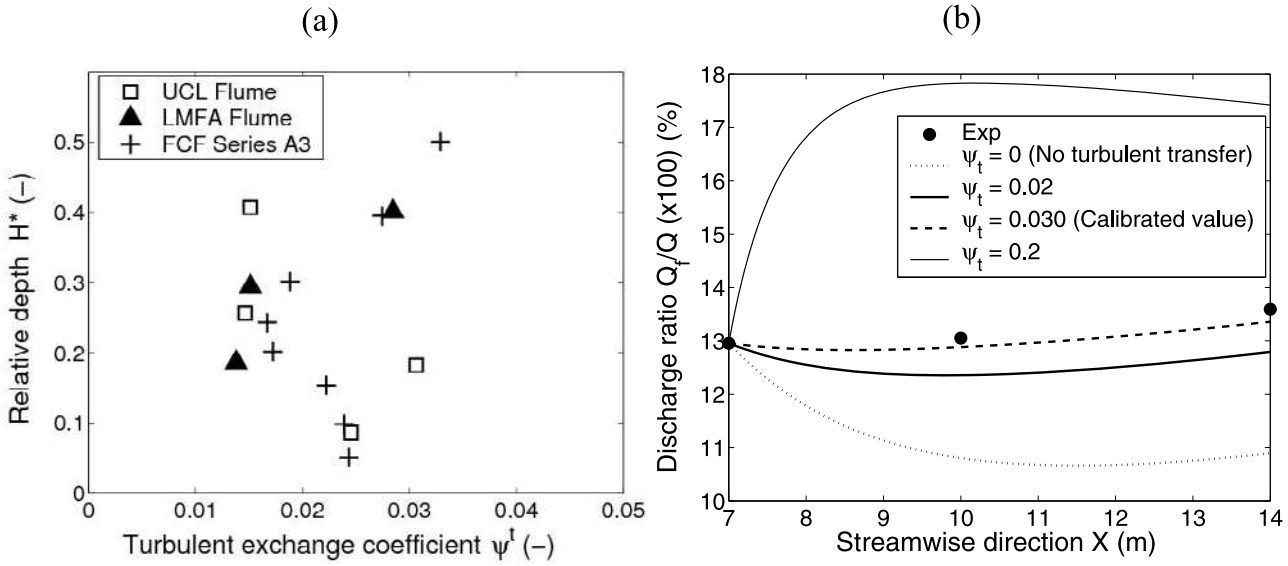

Figure 5. Turbulent exchange coefficient ψ^t. (a) Calibration under uniform flow conditions and (b) sensitivity of floodplain discharge Q_f using ISM with a mean value $\psi^t = 0.02$, UCL flume, $H^* = 0.18$.

diverging floodplains, with an abrupt floodplain contraction, and with symmetrically converging floodplain. In Table 3, relative depth measured at midlength of a reach with variable total width is denoted $H_{1/2}^*$. Typical lateral distributions of streamwise depth-averaged velocity U_d are presented in Figure 6. Considering the whole lateral profiles of velocity U_d, we clearly observed that the value of interface velocity strongly depends on the direction of mass transfer.

[28] First, the main tendency can be summarized as follows: with two subsections i and j parallel with regard to the longitudinal direction, their common interface velocity U_{int} approaches the average velocity U_i, when mass transfers occur from subsection i toward subsection j. Second, analyzing carefully the measured interface velocities, the following three cases have to be distinguished:

[29] 1. When the channel is prismatic and mass transfers occur from i toward j

$$U_{\text{int}} = U_i. \tag{13}$$

As shown in Figures 6a and 6b, equation (13) is consistent with flows in straight compound channel with an upstream floodplain discharge exceeding the discharge under uniform flow conditions.

[30] 2. When the compound geometry is nonprismatic and the overall channel width is constant

$$U_{\text{int}} = U_i \quad \text{if} \quad dB_i/dx < 0 \tag{14}$$

$$U_{\text{int}} = U_j \quad \text{if} \quad dBi/dx > 0. \tag{15}$$

As shown in Figure 6d, equations (14) and (15) are, respectively, relevant in the converging right-hand floodplain

Table 3. Nonuniform Flows[a]

	H^*	$H_{1/2}^*$	Q (L/s)
	Straight Geometries[b]		
UCL flume	0.09, 0.18, 0.27, 0.41		8, 10, 14, 24
LMFA flume	0.25–0.21, 0.34– 0.33, 0.34–0.33, 0.43–0.38		17.4, 24.7, 24.7, 36.3
CNR flume	0.21–0.19, 0.33–0.34		150, 260
	Skewed Geometries[c]		
Series A16 (5.1°)	0.145, 0.244, 0.407		230, 329, 686
Series A14 (5.1°)	0.148, 0.243, 0.408		261, 353, 725
Series A15 (9.2°)	0.146, 0.243, 0.408, 0.5		254, 356, 711, 1132
	Converging Geometries[d]		
Cv6 (3.8°)	0.21–0.11, 0.28–0.26, 0.30–0.20, 0.48–0.49, 0.48–0.47, 0.49–0.42	0.2, 0.3, 0.3, 0.5, 0.5, 0.5	10, 10, 12, 12, 16, 20
Cv2 (11.3°)	0.22–0.11, 0.27–0.25, 0.29–0.21, 0.47–0.48, 0.47–0.45, 0.49–0.41	0.2, 0.3, 0.3, 0.5, 0.5, 0.5	10, 10, 12, 12, 16, 20
Abrupt contraction (22°)	0.24–0.14, 0.42– 0.34	0.21, 0.41	150, 260
	Diverging Geometries[e]		
Dv6 (3.8°)	0.14–0.19, 0.22– 0.32, 0.18–0.34, 0.44–0.51, 0.27– 0.36, 0.40–0.52	0.2, 0.3, 0.3, 0.5, 0.3, 0.5	12, 12, 16, 16, 20, 20
Dv4 (5.7°)	0.11–0.25, 0.23– 0.34, 0.14–0.35, 0.45–0.52, 0.24– 0.39, 0.39–0.53	0.2, 0.3, 0.3, 0.5, 0.3, 0.5	12, 12, 16, 16, 20, 20

[a]Experimental data. Variation in relative depth H^* between upstream and downstream cross section, relative depth measured at midlength of the reach with variable width $H_{1/2}^*$, and total discharge Q. Note that relative depth $H_{1/2}^*$ is measured at $x = 5$ m for Cv6, Cv2, and Dv6; at $x = 4$ m for Dv4.
[b]*Proust* [2005] and *Bousmar et al.* [2005].
[c]*Sellin* [1993].
[d]*Bousmar et al.* [2004] and *Proust et al.* [2006a].
[e]*Proust* [2005] and *Bousmar et al.* [2006].

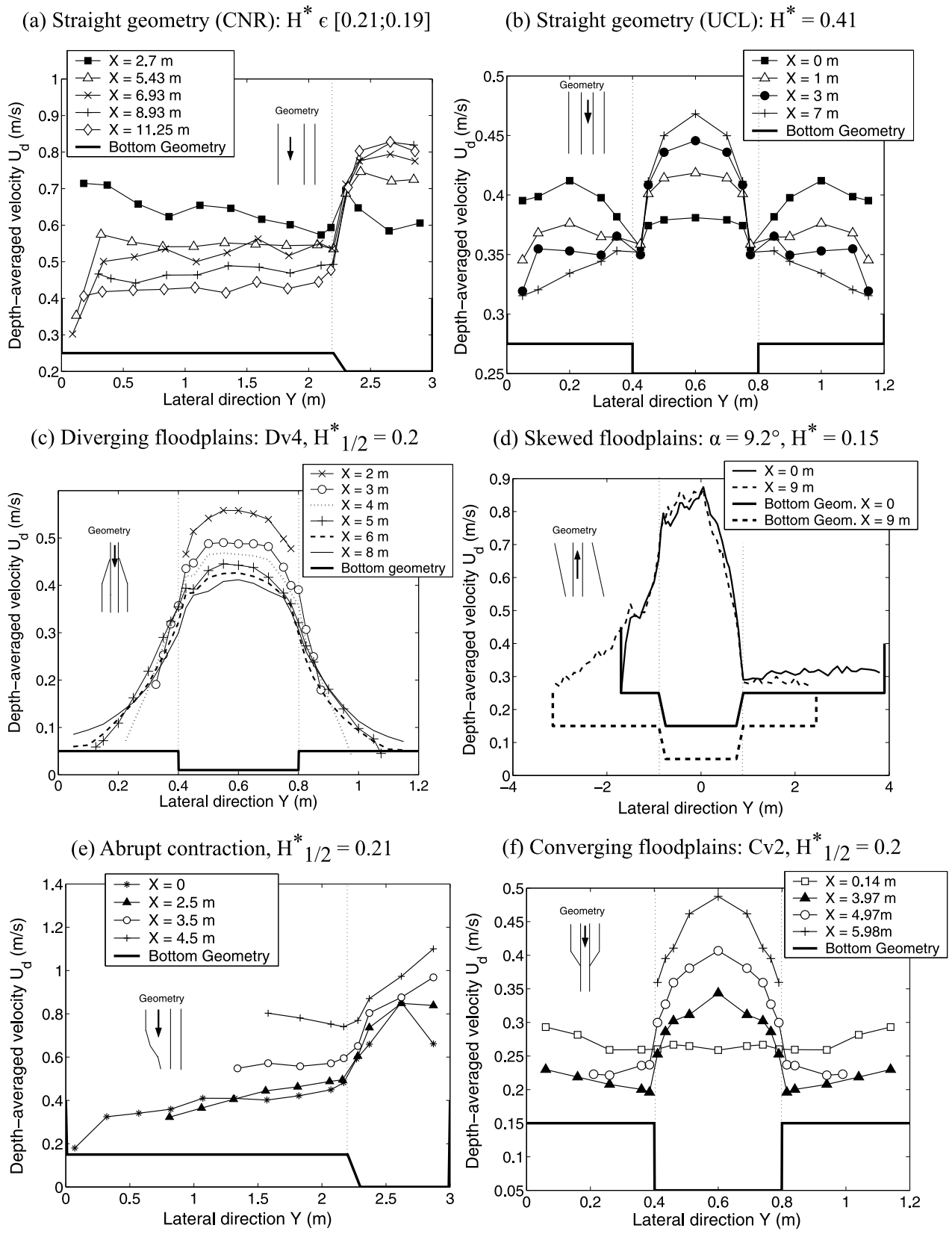

Figure 6. Typical lateral distributions of streamwise depth-averaged velocity U_d (experimental results).

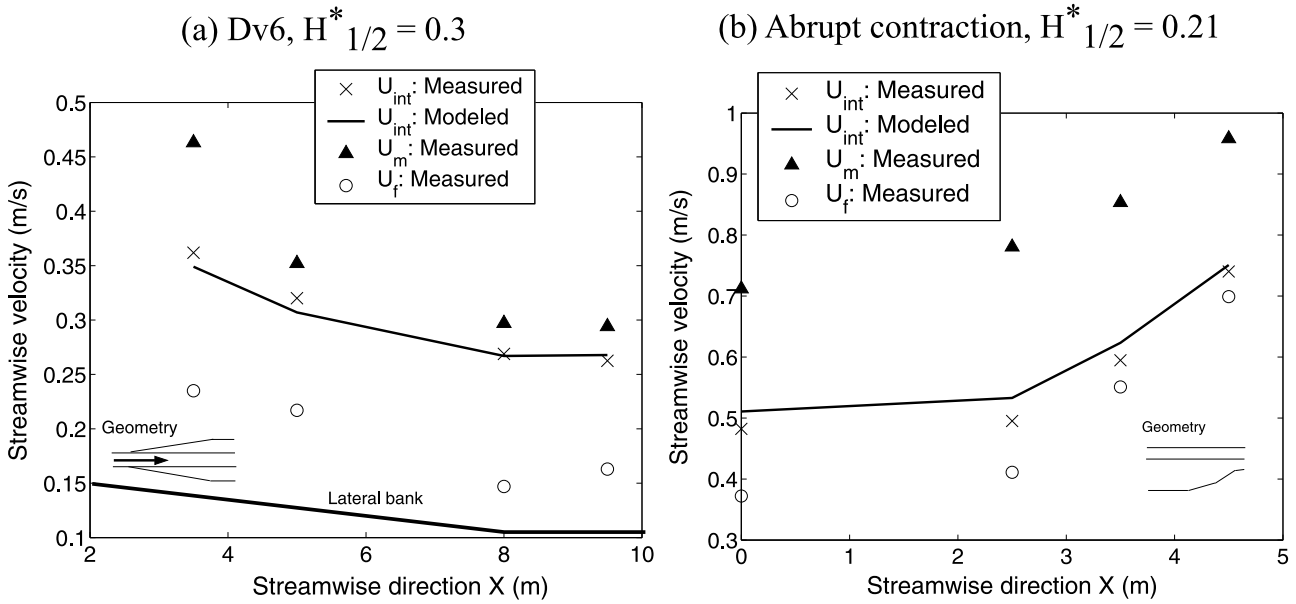

Figure 7. Streamwise depth-averaged velocity at the interfaces U_{int}. Modeled versus experimental values.

and in the diverging left-hand one of skewed compound channels (FCF Series A14, A15 and A16).

[31] 3. When the compound geometry is nonprismatic and the overall channel width is variable

$$U_{\mathrm{int}.l} = \varphi_l U_l + (1-\varphi_l)U_m \quad \text{and} \quad U_{\mathrm{int}.r} = \varphi_r U_r + (1-\varphi_r)U_m, \tag{16}$$

where φ_l and φ_r are weighting coefficients depending on the geometry.

[32] In equation (16), more weight is given to the floodplain velocity (U_l or U_r) in converging geometries, while more weight is given to the main channel velocity U_m in diverging geometries. Inspired by *Yen et al.* [1985], the coefficients φ_l and φ_r were determined by adjusting empirical formulas such as $U_{int.l}$ (or $U_{int.r}$) = f (B_i, B_j, U_i, U_j) from measured velocities U_m, U_l, U_r, $U_{int.l}$ and $U_{int.r}$. Equation (16) is in good agreement with experimental velocity using $\varphi_l = 4B_m/(4B_m + B_l)$ and $\varphi_r = 4B_m/(4B_m + B_r)$ in converging floodplains and abrupt floodplain contraction where $dB_f/dx < 0$ (Figures 6e and 6f), and with $\varphi_l = B_m/(B_m + 4B_l)$ and $\varphi_r = B_m/(B_m + 4B_r)$ in diverging floodplains where $dB_f/dx > 0$ (Figure 6c). These results are shown in Figure 7, where the modeled velocity U_{int} with equation (16) is compared to measured velocities U_{int}, U_m and U_f (U_l or U_r) for one asymmetric converging flow and one symmetrical diverging flow.

[33] To conclude, we used for ISM simulations: equation (13) for straight geometries; equations (14) and (15) for skewed geometries; and equation (16) for the 26 flows investigated in converging or diverging geometries (Dv4, Dv6, Cv2, Cv6, Abrupt floodplain contraction). By using these equations, we aimed at accurately model the momentum flux q_{lm}. $U_{int.l}$ and q_{rm}. $U_{int.r}$, in accordance with measured interface velocity. This modeling is a first stage of investigation of interface velocity for nonuniform flow. To extend these results to other types of geometries, further work should be devoted, notably to the weighting coefficients in equation (16) for geometry with variable width.

4. Three Types of Simulations

[34] In this preliminary investigation stage, the ISM is solved iteratively (see Appendix B), accounting for the measured upstream discharge distribution and downstream water level.

[35] Each momentum equation can alternatively be written as (according to equation (A2) in Appendix A)

$$S_{\mathrm{H}i} = -\frac{d\mathrm{H}_i}{dx} = S_{fi} \pm \frac{\tau_{ij} h_{\mathrm{int}}}{\rho g A_i} + \frac{q_{in}(U_i - U_{in}) + q_{out}(U_{out} - U_i)}{gA_i} = S_{fi} + S_i^t + S_i^m, \tag{17}$$

where H_i is subsection head is $Z_i + U_i^2/2g$, Z_i being water level in the subsection.

[36] In equation (17), the subsection head loss gradient is thereby the sum of bed friction slope S_{fi}, dissipation (or energy gain) due to interfacial turbulent shear stress τ_{ij} (denoted S_i^t), and dissipation (or energy gain) stemming from the momentum transfer due to lateral mass discharges q_{in} or q_{out} (denoted S_i^m). As slope S_{fi} is always positive but the two other terms can be either positive or negative, $S_{\mathrm{H}i} = -d\mathrm{H}_i/dx$ can represent a loss or a gain of head.

[37] To assess the influence of the different contributions to subsection head loss (or gain) $S_{\mathrm{H}i}$, the following three types of ISM simulations were carried out: (1) accounting for the total momentum transfer due to both turbulent diffusion and mass exchanges (equation (17); simulations (1) are labeled "$S_f + S^t + S^m$" in Figures 8–12); (2) only taking into account turbulent exchanges at the interfaces, i.e., $S_{\mathrm{H}i} = S_{fi} + S_i^t$ (simulations (2) are labeled "$S_f + S^t$"); and (3) ignoring the momentum transfer at the interfaces, i.e.,

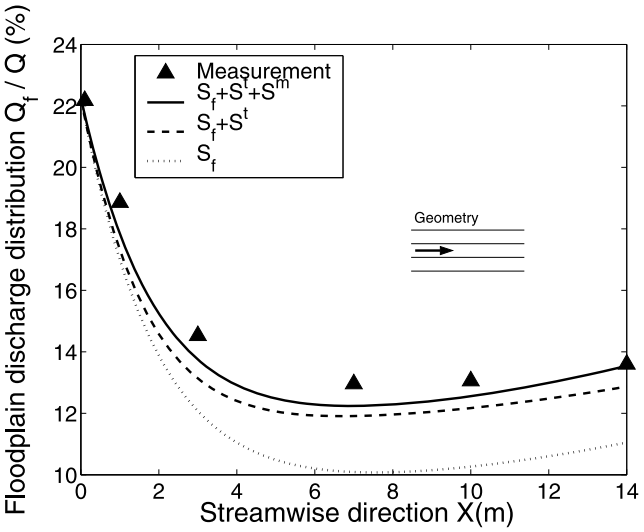

Figure 8. Straight compound channel. ISM simulations versus experimental data of floodplain discharge Q_f (as percentage of total discharge Q), UCL flume, relative depth H^* = 0.18.

considering bed friction as the only source of dissipation, i.e., $S_{Hi} = S_{fi}$ (simulations (3) are labeled "S_f").

5. ISM Validation

[38] The Independent Subsections Method was tested against measurements from the various data sets presented in Table 3: developing flows in straight compound channel [*Bousmar et al.*, 2005; *Proust*, 2005], flows in skewed compound channel [*Sellin*, 1993], in a symmetric converging compound channel [*Bousmar et al.*, 2004], in a symmetric diverging geometry [*Proust*, 2005; *Bousmar et al.*, 2006], and in an asymmetrical compound channel with an abrupt floodplain contraction [*Proust et al.*, 2006a]. In all, 11 geometries and 61 different flow configurations were used to evaluate the ISM: 15 uniform flows and 46 nonuniform flows, for relative depth H^* in the range 0.05 to 0.53. Maximum relative errors between ISM results and experimental data are presented in Table 4.

5.1. Developing Flows in Straight Compound Channels

[39] Developing flows investigated here are characterized by an unbalanced upstream discharge distribution, giving rise to mass transfers from the floodplain(s) toward the main channel (see Figures 6a and 6b). Depending on the geometrical and hydraulic parameters, the flow may be (or not) far from uniformity in the downstream part of the reach concerned, due to limited flume length. These flows also present low or no variation in flow depth in the streamwise direction.

[40] ISM simulations of floodplain discharge Q_f is presented in Figure 8 for one UCL flow with relative depth H^* = 0.18. ISM satisfactorily reproduces changes in the floodplain discharge only when the total momentum transfer is taken into account (maximum relative error lower than 4%). On the other hand, ignoring both mass and turbulent exchanges in the momentum transfer leads to a 20% underestimation of the floodplain discharge at the downstream end of the reach concerned (station x = 14 m).

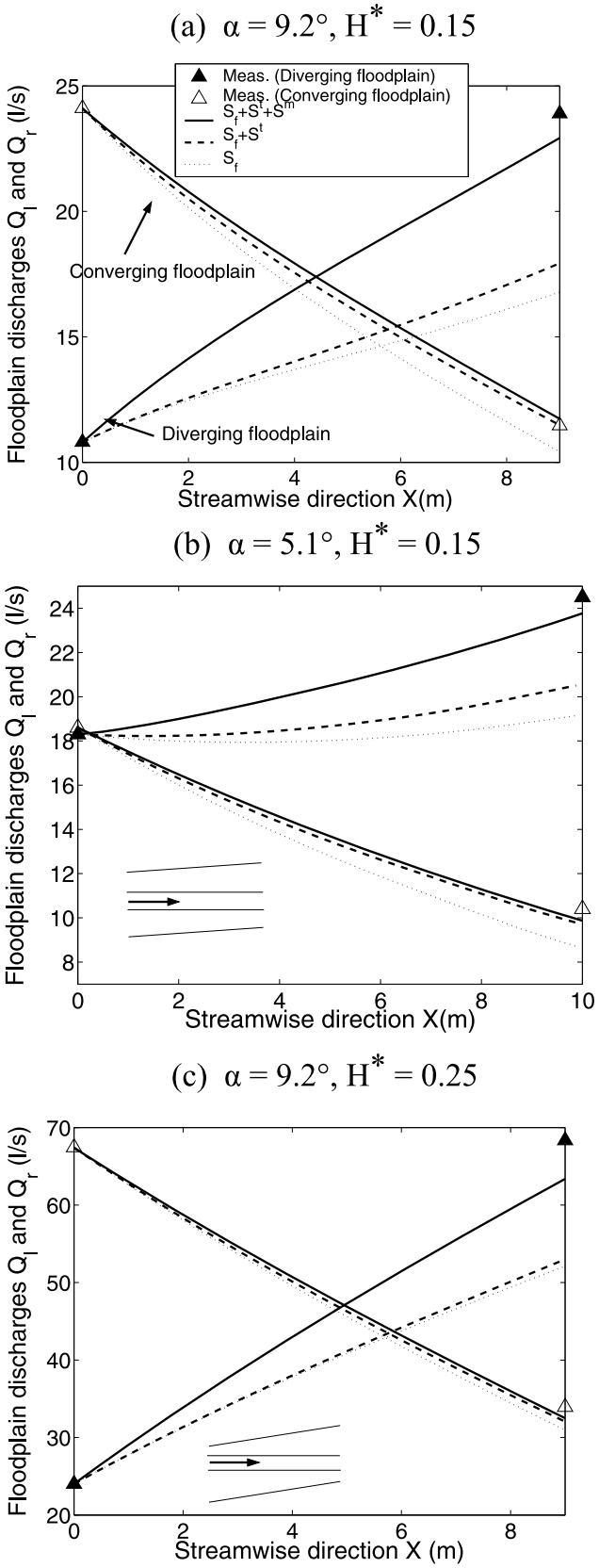

Figure 9. Skewed floodplains. ISM simulations of discharges in the left and the right floodplains (Q_l and Q_r) against experimental data (Series A15 and A16).

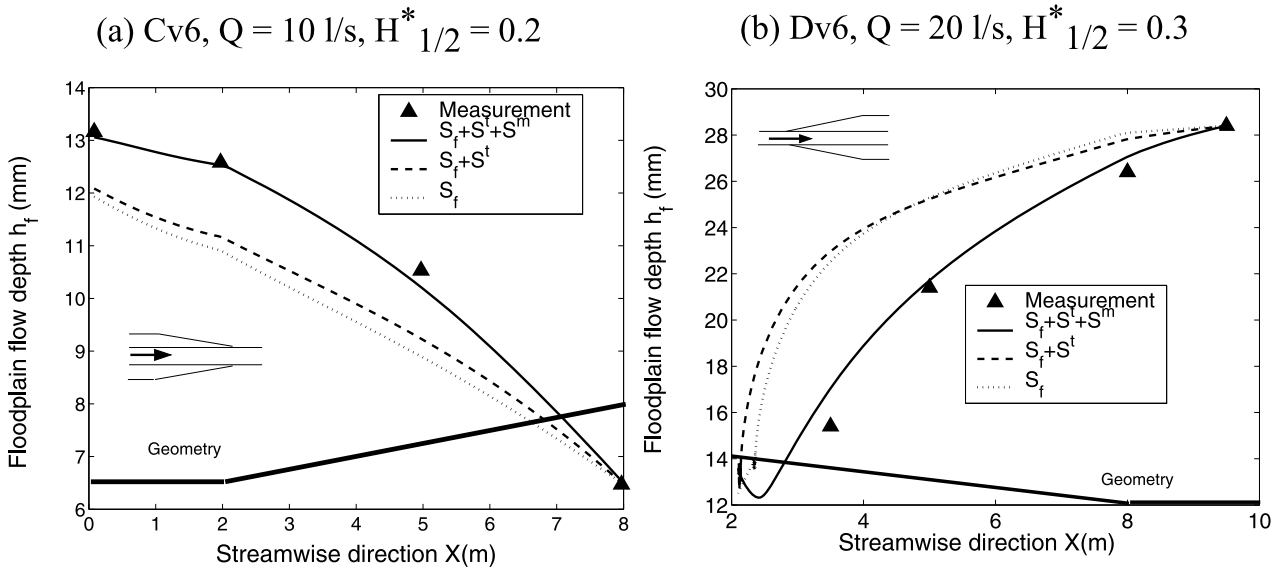

Figure 10. ISM results versus experimental measurements of flow depth in the floodplain h_f in symmetric converging and diverging floodplains Cv6 (α = 3.8°) and Dv6 (α = 3.8°).

Figure 8 also indicates that turbulence plays a predominant role in lateral momentum transfer for straight channels. Correct modeling of turbulent transfer is necessary to obtain the correct discharge distribution when the flow tends to uniformity in the downstream part of the reach. Similar results were obtained for the other nonuniform flows in the UCL straight geometry: the lateral momentum flux is far more controlled by the turbulent exchange than by the mass exchanges. Results not shown here evidence the fact that the effect of dissipation S^t decreases with increasing relative depth H^*. For $H^* = 0.4$, accounting for the head loss due to turbulent exchange S^t has no effect on the ISM simulations.

[41] The computed flow depths are not represented here because of the very small variations from upstream to downstream boundaries: less than 1 mm in the UCL flume, and inferior to 3 mm in the CNR flume. They are in good agreement with the experimental data (maximum error of −6%). Unlike the discharge distribution, the computed water surface profiles are not influenced by turbulent exchange when approaching uniform flow conditions: the three simulation types are similar.

[42] The maximum relative error in the floodplain discharge computation is +15% (see Table 4). It was obtained for a CNR flow. This could be due to the slight curvature of the CNR flume (see Figure 2f), which increases the mass transfer toward the main channel more noticeable and which is not taken into consideration in the modeling.

5.2. Skewed Compound Channels

[43] Skewed flow experiments are particularly interesting for ISM validation, since the diverging left-hand floodplain and the converging right-hand floodplain have opposite behaviors when considering the direction of mass transfer (see Figure 6d).

[44] For the 3 geometries and the 10 flow configurations investigated (see Table 3), ISM computes discharge Q_l or Q_r with a maximum error of 7% when considering the total momentum exchange. It also reproduces the observed flow depth profile (max. error of +1%) with no variation between the upstream and downstream boundaries. Indeed, variations of computed flow depth are less than 1 mm, i.e., less than 0.6% of the main channel flow depth.

[45] Computed and experimental discharges Q_l or Q_r on the left and right floodplains are presented in Figure 9, for two geometries (Series A15, α = 9.2°, main channel side slope s = 1:1; Series A16, α = 5.1°, s = 0) and two relative depths (H^* = 0.15, 0.25). A clear asymmetry of the effect of momentum transfer is observed between the narrowing right floodplain and the enlarging left one. This could be expected from observations of the lateral gradients of depth-averaged velocities U_d over the two floodplains (Figure 6d): nil on the converging floodplain and significant on the enlarging one. The influence of momentum transfer due to mass exchange is significant on the diverging floodplain, goes up with an increasing α angle and decreases with rising relative depth H^*. In contrast, the effect of dissipation S^m is nil on the converging floodplain. Regarding momentum transfer due to turbulent diffusion, a very slight influence is observed on the two floodplains for the smallest relative depth. The latter result is consistent with experimental momentum balances obtained by *Elliot and Sellin* [1990]. They showed that the influence of turbulent transfer decreases rapidly with an increase in mass transfer between subsections. ISM results not shown here demonstrate that the total momentum transfer (and associated S^m and S^t) has no influence on hydraulic parameters for relative depth H^* equal to 0.4 on the two interfaces.

[46] Finally, ISM results prove that the discharge distribution is significantly influenced by momentum due to mass exchange through the left interface (diverging floodplain) for small and medium relative depths (H^* = 0.15 and 0.25), and to a lesser extent, by momentum due to turbulent diffusion through the two interfaces only for H^* = 0.15. These phenomena are reinforced when the skewness angle α increases, but are not sensitive to the slope of the main channel banks (comparing series A16 and A14).

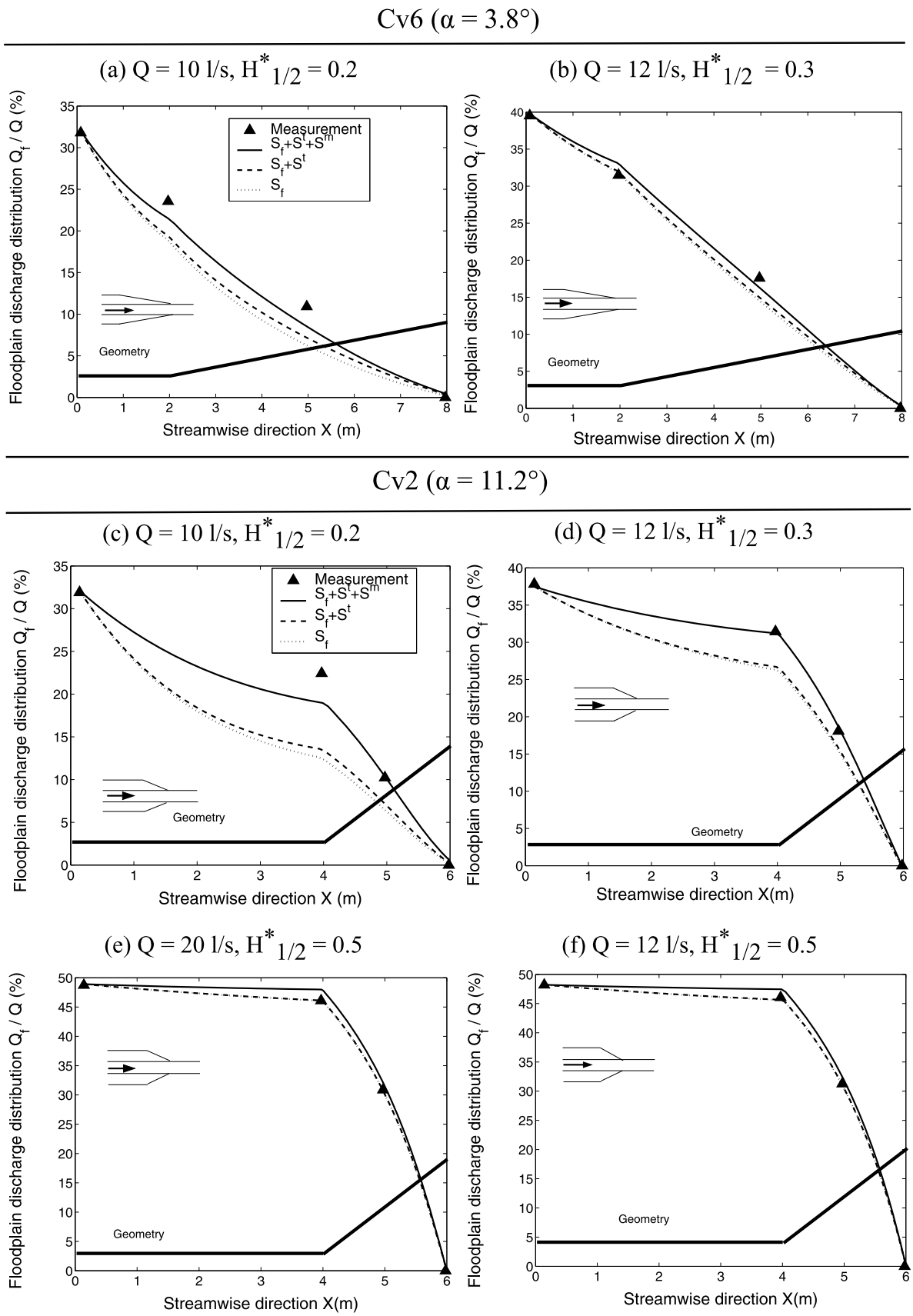

Figure 11. Symmetric converging floodplains (Cv2 and Cv6). ISM simulations versus experimental measurements of floodplain discharge Q_f (as percentage of total discharge Q).

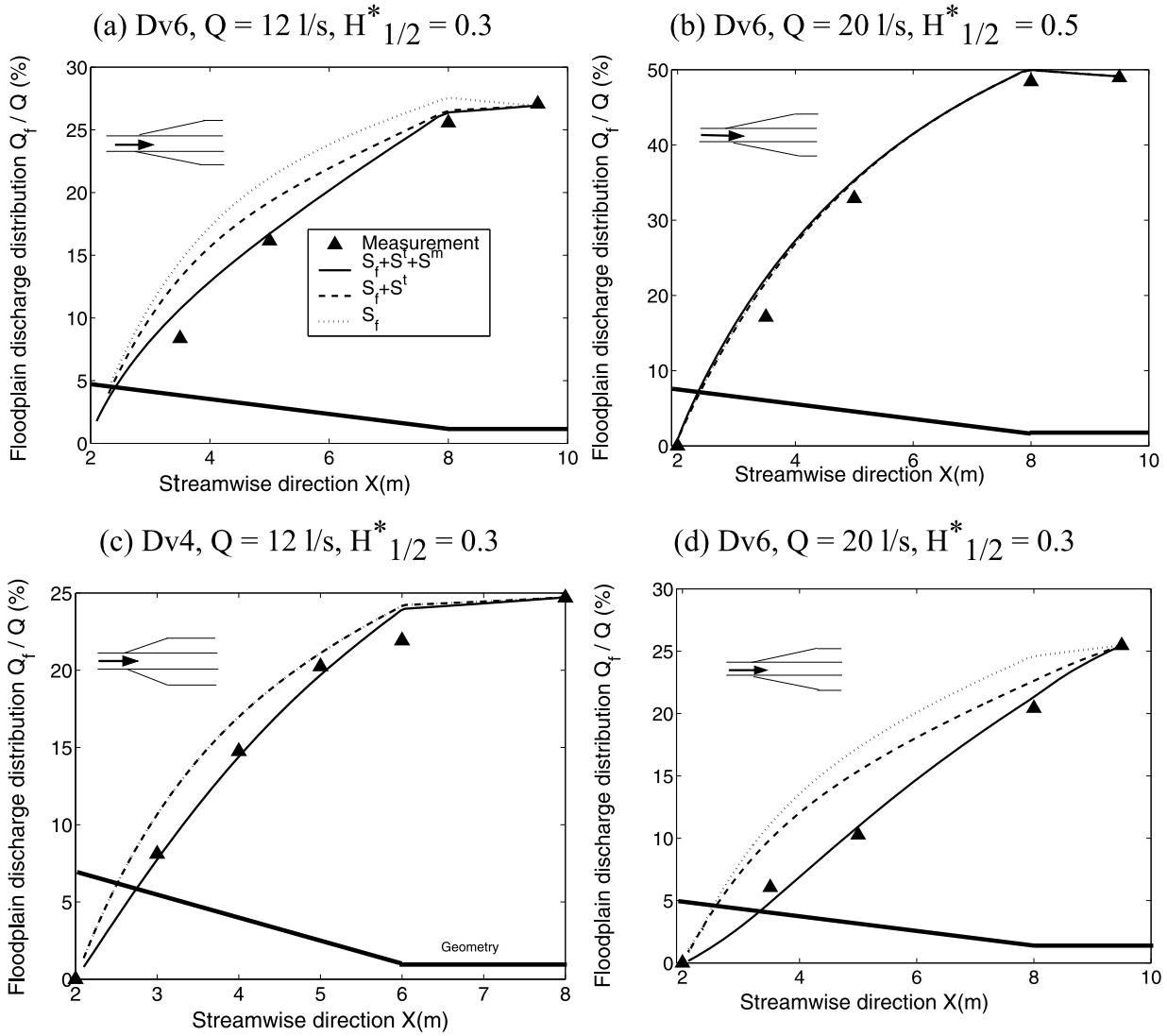

Figure 12. Symmetrically diverging floodplains Dv6 (3.8°) and Dv4 (5.7°). ISM simulations of floodplain discharge Q_f (as percentage of total discharge Q) versus experimental data.

5.3. Symmetrically Converging Floodplains

[47] Figure 10a presents the floodplain flow depth h_f for a small overbank flow in Cv6. Floodplain discharge Q_f, sum of Q_l and Q_r is shown in Figure 11 for 6 runs, chosen to emphasize the role on flow physics of relative depth H^*, angle α, and of total discharge Q. Figures 11a–11f show that mass exchanges have far more influence than turbulence on the interfacial momentum flux (see notably 11c and 11d). This situation contrasts with developing flows in straight

Table 4. ISM Results[a]

Geometry	Considering $S_f + S^t + S^m$		Considering $S_f + S^t$		Considering S_f	
	h_f (%)	Q_l or Q_r (%)	h_f (%)	Q_l or Q_r (%)	h_f (%)	Q_l or Q_r (%)
Straight CNR (nonuniform flow)	2	15	5	15	5	15
Straight UCL (nonuniform flow)	6	4	6	9	6	20
Straight LMFA (nonuniform flow)	6	11	6	11	10	14
Skewed (5.1°), FCF Series A14 and A16	1	4	3	16	3	22
Skewed (9.2°), FCF Series A15	1	7	3	25	3	30
Abrupt contraction (22°)	8	8	15	11	15	11
Converging Cv6 (3.8°)	4	19	10	39	13	46
Converging Cv2 (11.2°)	4	13	19	41	21	44
Diverging Dv4 (5.7°)	8	8	22	78	22	78
Diverging Dv6 (3.8°)	6	16	45	55	43	122

[a]Maximum relative errors on floodplain flow depth h_f and floodplain discharges Q_l or Q_r, considering one, two, or three sources of head loss.

compound channels (see section 5.1), for which dissipation S^m was negligible compared to dissipation S^t.

[48] Furthermore, the effect of momentum flux due to mass exchange increases when angle α increases. This flux is also more sensitive to a change in relative depth (for a given discharge Q) than to a change in total discharge (for a given range of relative depth). For high relative depth $H_{1/2}^* = 0.5$, the momentum transfer due to mass exchange has a negligible influence on the ISM simulations. On the other hand, this flux significantly influences the computation of flow depth and discharge in the floodplain for the two shallow overbank flows ($H_{1/2}^* = 0.2$), as shown, e.g., in Figure 10a and in Figure 11c.

[49] Maximum discrepancies between ISM results and experimental data are reported in Table 4 for the two geometries Cv2 and Cv6. When the whole momentum transfer at the interfaces is accounted for, relative errors in floodplain flow depth h_f are less than 4% for all the flows investigated. The simulations of floodplain discharge Q_f accurately matches the experimental measurements for the flows with relative depth $H_{1/2}^* = 0.3$ and 0.5. For the two small overbank flows ($H_{1/2}^* = 0.2$), the floodplain discharge is underestimated by −13% (Cv2) and −19% (Cv6). Finally, ISM results clearly demonstrate that momentum transfer due to mass exchanges should be considered for overbank flows with relative depth $H_{1/2}^*$ less than 0.3 when attempting to model both flow depth and discharge distribution in narrowing reaches of this type.

5.4. Symmetrically Diverging Floodplains

[50] The flows in diverging floodplains Dv6 (3.8°) and Dv4 (5.7°) were also investigated according to ISM results. Figure 10b shows the flow depth in the floodplain for a medium relative depth $H_{1/2}^*$ in Dv6 and Figure 12 presents the floodplain discharge Q_f for 4 runs. As in converging floodplains, the influence of momentum flux due to mass exchange is important for medium and small relative depths. However, this flux plays an opposite role in diverging geometry since this reduces both the flow depth and the discharge in the floodplain. In the downstream prismatic part, a slight influence of turbulent diffusion is highlighted for the smaller angle α (Dv6) and relative depth $H_{1/2}^*$ lower than 0.3. For flows with high discharge and medium relative depth, *Proust et al.* [2008] show that the head slope gradient in the floodplain is negative: the energy term S_f^m (energy gain) enables the floodplain-averaged head to be increased.

[51] The ISM simulates the water surface with a maximum relative error of 8% in the two diverging geometries (Table 4). For flow with high discharge and moderate relative depths, the modeling of the floodplain flow depth h_f is very sensitive to lateral momentum flux: in Figure 10b, only accounting for bed friction ("S_f curve") results in a +43% overestimation in flow depth h_f. For flows with lower discharge and/or higher relative depth, water surface profiles are less influenced by interfacial processes than is the evolution of discharge distribution.

[52] Regarding the floodplain discharge Q_f, the maximum relative error is 16% in Dv6 and 8% in Dv4 when considering the whole momentum flux at the interface. When no momentum transfer is taken into account, these errors increase to +122% and +78% in Dv6 and Dv4, respectively. Moreover, in contrast to flow in symmetrically converging floodplains, the momentum flux at the interfaces is sensitive to an increase in total discharge Q (for a given relative depth $H_{1/2}^*$). When the flow enters the diverging compound channel, increasing discharge Q accentuates the difference in subsection velocities $U_m - U_f$. Consequently, interfacial momentum flux and associated energy terms S^m and S^t rise. However, the effect of this flux vanishes at high relative depth, as shown in Figure 12b.

5.5. Abrupt Floodplain Contraction

[53] ISM simulations were also conducted for flows in the compound channel with an abrupt contraction of the floodplain ($\alpha = 22°$, see Figure 3e). The computed flow depth and mean velocity in the floodplain are presented in Figure 1 when considering the total momentum transfer, for $H_{1/2}^* = 0.21$. Though mass transfers become severe in this geometry, ISM still correctly predicts both profiles of water surface and floodplain velocity. Simulations not illustrated here confirm the above conclusions for symmetrically narrowing floodplains: momentum flux related to mass exchange was found to have a notable influence on the flow depth and floodplain discharge for shallow overbank flow ($H_{1/2}^* = 0.21$) in converging geometry.

[54] Using this challenging flow case for comparing the ISM to the classical DCM, to a corrected DCM and to the EDM leads to a primordial result. Figure 1 shows that a 1-D equation defined on the total cross section cannot simultaneously predict both water level and discharge distribution satisfactorily. The interest of computing the water surface profile in each subsection with the ISM is thus demonstrated.

6. Conclusion

[55] A new 1-D methodology, called Independent Subsections Method, was developed to model nonuniform flows in compound channel. This method predicts two parameters of interest to engineers: flow depth and mean velocity in floodplains. Unlike 1-D common models (such as DCM, corrected DCM or EDM), ISM computes the water surface profile on each subsection (main channel, left-hand and right-hand floodplain). This enables the water level and the three subsection mean velocities to be simultaneously calculated, without giving priority to any variable. In opposition to the three other 1-D approaches, the ISM assumes independent evolution of the discharge in each subsection, since this method does not assume equal head loss gradients in all subsections, and it does not impose subsection discharges at the downstream boundary. The ISM explicitly models mass conservation and momentum conservation at the interfaces between parallel subsections. Momentum transfer is separated into two contributions: momentum flux due to turbulent diffusion, and momentum flux due to mass exchange. The method was validated against experimental data for: developing flows in straight compound channel, flows in channel with skewed floodplain boundaries, and with converging and diverging floodplains. The maximum relative errors in the calculation of the couple {flow depth, discharge} in the floodplain are {−8%;−19%} for the 46 runs investigated. By distinguishing three different sources of head loss, the ISM appears to be a useful theoretical tool to improve our understanding of physical processes governing compound channel flows. Comparing ISM calculations with experimental measurements leads to the following conclusions:

[56] 1. In all geometries, water surface profiles are less sensitive to momentum transfer between subsections than is the discharge distribution across the channel.

[57] 2. Turbulent exchanges are predominant in the momentum transfer in straight geometry, only when the flow is approaching equilibrium.

[58] 3. Momentum transfer is mainly controlled by mass exchanges in nonprismatic channels.

[59] 4. For skewed flow experiments, the influence of lateral momentum transfer is asymmetrical in the two floodplains: the discharge distribution is significantly influenced by momentum due to mass exchange through the left interface (diverging floodplain) for relative depth $H^* \leq 0.25$, and to a lesser extent, by momentum due to turbulent diffusion through the two interfaces only for $H^* = 0.15$.

[60] 5. In symmetrically converging floodplains, momentum transfer due to mass exchanges should be considered for overbank flows with relative depth H^* less than 0.3.

[61] 6. In symmetrically diverging floodplains, momentum flux caused by mass exchange reaches high values in the floodplains for $H^* \leq 0.4$. In particular, this transfer enables the floodplain-averaged head to be increased for flows with high discharge and medium relative depth.

Appendix A: ISM Equations

[62] Considering that

$$-\frac{1}{gA_i}\frac{d}{dx}\left(A_i U_i^2\right) = -\frac{U_i}{gA_i}\frac{dA_i U_i}{dx} - \frac{U_i}{g}\frac{dU_i}{dx}, \qquad \text{(A1)}$$

including equation (A1) in equation (1), and taking into account the mass conservation equation (2), gives

$$S_{fi} = -\frac{dZ_i}{dx} - \frac{U_i}{g}\frac{dU_i}{dx} \pm \frac{\tau_{ij}.h_{\text{int}}}{\rho g A_i} + \frac{q_{in}(U_{in} - U_i) + q_{out}(U_i - U_{out})}{gA_i}, \qquad \text{(A2)}$$

where Z_i is water level in the subsection, and $dZ_i/dx = dh_i/dx - S_o$

[63] Developing the mass conservation equation (2) multiplied by $U_i/(gA_i)$ leads to

$$\frac{U_i}{g}\frac{dU_i}{dx} + \frac{U_i^2}{gA_i}\frac{dA_i}{dx} = \frac{(q_{in} - q_{out})}{gA_i}U_i. \qquad \text{(A3)}$$

With $A_i = B_i.h_i$, equation (A3) gives

$$-\frac{U_i}{g}\frac{dU_i}{dx} = \frac{(q_{out} - q_{in})}{gA_i}U_i + \frac{U_i^2}{gh_i}\frac{dh_i}{dx} + \frac{U_i^2}{gB_i}\frac{dB_i}{dx}. \qquad \text{(A4)}$$

Including equation (A4) in equation (A2) gives

$$\frac{dh_i}{dx}\left(1 - \frac{U_i^2}{gh_i}\right) = S_0 - S_{fi} + \frac{U_i^2}{gB_i}\frac{dB_i}{dx} \pm \frac{\tau_{ij}.h_{\text{int}}}{\rho g A_i} + \frac{q_{in}(U_{in} - 2U_i) + q_{out}(2U_i - U_{out})}{gA_i}. \qquad \text{(A5)}$$

[64] Note that at this first stage of development of ISM, only rectangular subsections were considered ($A_i = B_i \times h_i$) to simplify the equations. With bed level changes in a subsection, ISM equations should be developed considering the wetted perimeter P_i and the hydraulic radius R_i, with $A_i = P_i \times R_i$.

Appendix B: ISM Solving

[65] For flows in straight compound channels, *Yen et al.* [1985] proposed the simultaneous solving of the quadruplet $\{dh_l/dx; dQ_l/dx; dQ_m/dx; dQ_r/dx\}$ by using either an explicit or an implicit method. For nonprismatic compound channels, the formulation of the equations system is simplified by solving the quadruplet $\{dh_l/dx; dU_l/dx; dU_m/dx; dU_r/dx\}$ with an explicit method. For the sake of conciseness, the final system of the three 1-D momentum equations and the mass conservation can be expressed in matrix form [see *Proust*, 2005, pp.141–143] as follows:

$$A(Y).\frac{dY}{dx} = F(Y) \qquad \text{with} \qquad Y = \begin{pmatrix} h_l \\ U_l \\ U_m \\ U_r \end{pmatrix}, \qquad \text{(B1)}$$

where coefficients of A and F matrix are nonlinear functions of velocities U_l, U_r, U_m, flow depth h_l, geometrical parameters and subsection Manning roughness, with $h_l = h_r = h_m - h_b$.

[66] For subcritical flows, the ISM is solved iteratively: the measured upstream discharge distribution and a tentative upstream water level are given. A corresponding value of the downstream water level results from the computation. The upstream level is then adjusted until the appropriate downstream level is obtained, keeping the upstream discharge distribution constant. In the future, more efficient numerical developments will be carried out.

Notations

A_i	subsection area.
B	total width.
B_i	subsection width.
h_b	bank full flow depth in the main channel.
h_i	subsection flow depth.
H^*	relative flow depth.
$H_{1/2}^*$	relative flow depth at midlength of diverging or converging reach.
H_i	subsection head.
n	Manning roughness.
q_{in}	lateral inflow per unit length.
q_{out}	lateral outflow per unit length.
q_{rm}	lateral mass discharge between the right floodplain and the main channel (algebraic value).
q_{lm}	lateral mass discharge between the left floodplain and the main channel (algebraic value).
Q	total discharge.
R_h	hydraulic radius.
S_0	bed slope.
S_{fi}	subsection friction slope.
S_{Hi}	subsection head loss gradient.
U_d	depth-averaged velocity in the x direction.
U_i	subsection mean velocity.
U_{in}	longitudinal velocity of lateral inflow q_{in} at the interface.

$U_{int.l}$ longitudinal velocity at the interface between the left floodplain and the main channel.
$U_{int.r}$ longitudinal velocity at the interface between the right floodplain and the main channel.
U_{out} longitudinal velocity of lateral outflow q_{out} at the interface.
x longitudinal direction.
y lateral direction.
Z water level above reference datum.
α angle between the floodplain lateral walls and the main channel axis (x direction).
α_i Coriolis coefficient in subsection i.
βi Boussinesq coefficient in subsection i.
τ_{ij} shear stress at the vertical interface between two parallel subsections i and j along x axis (depth-averaged value).
ψ^t coefficient of turbulent exchange.

Subscripts

f floodplain.
i a subsection ($i = l$, r or m).
l left-hand floodplain.
m main channel.
r right floodplain.

[67] **Acknowledgments.** Experiments in CNR flume, UCL flume, and LMFA flume were funded by research programmes PNRH 99–04 and ECCO-PNRH 05CV123. D. Bousmar, N.Rivière, and S. Proust travel costs were supported by the Tournesol program grant 02947VM, funded by EGIDE, France, and CGRI, Communauté Française de Belgique, Belgium.

References

Ackers, P. (1993), Flow formulas for straight two-stage channels, *J. Hydraul. Res.*, *31*(4), 504–531.

Bousmar, D. (2002), Flow modelling in compound channels. Momentum transfer between main channel and prismatic or non-prismatic floodplains, Ph.D. thesis, 306 pp., Univ. Cath. de Louvain, Louvain-la-Neuve, France.

Bousmar, D., and Y. Zech (1999), Momentum transfer for practical flow computation in compound channels, *J. Hydraul. Eng.*, *125*(7), 696–706, doi:10.1061/(ASCE)0733-9429(1999)125:7(696).

Bousmar, D., N. Wilkin, J. H. Jacquemart, and Y. Zech (2004), Overbank flow in symmetrically narrowing floodplains, *J. Hydraul. Eng.*, *130*(4), 305–312, doi:10.1061/(ASCE)0733-9429(2004)130:4(305).

Bousmar, D., N. Rivière, S. Proust, A. Paquier, R. Morel, and Y. Zech (2005), Upstream discharge distribution in compound-channel flumes, *J. Hydraul. Eng.*, *131*(5), 408–412, doi:10.1061/(ASCE)0733-9429(2005)131:5(408).

Bousmar, D., S. Proust, and Y. Zech (2006), Experiments on the flow in a enlarging compound channel, in *River Flow 2006: Proceedings of the International Conference on Fluvial Hydraulics, Lisbon, Portugal, 6–8 September 2006*, edited by R. M. L. Ferreira et al., pp. 323–332, Taylor and Francis, Leiden, Netherlands.

Elliot, S. C. A., and R. H. J. Sellin (1990), SERC flood channel facility: Skewed flow experiments, *J. Hydraul. Res.*, *28*(2), 197–214.

Ervine, D. A., and J. I. Baird (1982), Rating curves for rivers with overbank flow, *ICE Proc.*, *73*, 465–472.

Huthoff, F., P. C. Roos, D. C. M. Augustijn, and S. J. M. H. Hulsher (2008), Interacting divided channel method for compound channel flow, *J. Hydraul. Eng.*, *134*(8), 1158–1165, doi:10.1061/(ASCE)0733-9429(2008)134:8(1158).

Knight, D. W. (1992), SERC flood channel facility: Experimental data—Phase A, *Rep. SR 314*, HR Wallingford Ltd., Wallingford, U. K.

Lambert, M. F., and R. H. J. Sellin (1996), Discharge prediction in straight compound channels using the mixing length concept, *J. Hydraul. Res.*, *34*(3), 381–394.

Martin-Vide, J. P., and P. J. M. Moreta (2008), Formulae for apparent shear stress in straight compound channels with smooth floodplains, in *River Flow 2008: Proceedings of the International Conference on Fluvial Hydraulics Cesme-Izmir, Turkey, 3–5 September 2008*, edited by M. S. Altinakar et al., pp. 465–476, Congr. Dep. and Travel Serv., Ankara.

Martin-Vide, J. P., P. J. M. Moreta, and S. Lopez-Querol (2008), Improved 1-D modelling in compound meandering channels with vegetated floodplains, *J. Hydraul. Res.*, *46*(2), 265–276.

Nicollet, G., and M. Uan (1979), Ecoulements permanents à surface libre en lit composés, *Houille Blanche*, *1*, 21–30.

Proust, S. (2005), Ecoulements non-uniformes en lits composés: Effets de variations de largeur du lit majeur, Ph.D. thesis, 362 pp., INSA Lyon, Lyon, France. (Available at http://cemadoc.cemagref.fr/cemoa/PUB00018439)

Proust, S., N. Rivière, D. Bousmar, A. Paquier, Y. Zech, and R. Morel (2006a), Flow in compound channel with abrupt floodplain contraction, *J. Hydraul. Eng.*, *132*(9), 958–970, doi:10.1061/(ASCE)0733-9429(2006)132:9(958).

Proust, S., D. Bousmar, N. Rivière, A. Paquier, and Y. Zech (2006b), A methodology for computing non-uniform flows in compound channels, in *River Flow 2006: Proceedings of the International Conference on Fluvial Hydraulics, Lisbon, Portugal, 6–8 September 2006*, edited by R. M. L. Ferreira et al., pp. 405–414, Taylor and Francis, Leiden, Netherlands.

Proust, S., A. Paquier, N. Rivière, and D. Bousmar (2008), Resolving energy losses for non-uniform flows in compound channel, in *River Flow 2008: Proceedings of the International Conference on Fluvial Hydraulics Cesme-Izmir, Turkey, 3–5 September 2008*, edited by M. S. Altinakar et al., pp. 437–445, Congr. Dep. and Travel Serv., Ankara.

Sellin, R. H. J. (1993), SERC flood channel facility: Experimental data—Phase A: Skewed floodplain boundaries, *Rep. Bristol BS8 1TR*, Univ. of Bristol, Bristol, U. K.

Yen, B. C. (1984), Hydraulics of flood plains: Methodology for backwater computation, *Wiss. Ber. 84/5*, Inst. für Wasserbau, Stuttgart, Germany.

Yen, B. C., R. Camacho, R. Kohane, and B. Westrich (1985), Significance of flood plains in backwater computation, paper presented at International Association of Hydro-Environment Engineering and Research 21st Congress, Melbourne, Victoria, Australia, 19–23 Aug.

D. Bousmar, Laboratoire de Recherche Hydraulique, Service Public de Wallonie, Rue de l'Abattoir 164, B-6200 Châtelet, Belgium. (didier.bousmar@spw.wallonie.be)

A. Paquier and S. Proust, Unité de Recherche Hydrologie-Hydraulique, Cemagref, 3 Bis Quai Chauveau CP220, F-69336 Lyon CEDEX 09, France. (andre.paquier@camagref.fr; sebastien.proust@cemagref.fr)

N. Riviere, Laboratoire de Mécanique des Fluids et d'Acoustique, UMR5509, CNRS, INSA de Lyon, Bat Jacquard, 20 Ave. A Einstein, F-69621 Villeurbanne, France. (nicolas.riviere@insa-lyon.fr)

Y. Zech, Unité de Génie Civil, Université Catholique de Louvain, Place du Levant 1, B-1348 Louvain-la-Neuve, Belgium. (yves.zech@uclouvain.be)